npj | climate and atmospheric science

Perspective

Published in partnership with CECCR at King Abdulaziz University

https://doi.org/10.1038/s41612-024-00589-2

# The influence of subpolar marine ice expansion on global climate in the Early Pleistocene



Wenxia Han[1,2] ✉, Jinbo Zan[3] ✉, David B. Kemp[4], Tao Zhang[5], Zhixiang Wang[1], Li Mai[1] & Xiaomin Fang[3]

Major climatic-environmental transitions and ecological shifts occurred during the mid-Early Pleistocene, a time when external forcing conditions were relatively stable. To help elucidate their driving mechanisms, we perform linear-nonlinear analysis on global climate and oceanographic records. A synchronous change in these records, starting at 1.9–1.6 Ma, was accompanied by an increased obliquity signal and coeval climate regime shifts. We posit that bipolar cooling and an extension of terrestrial ice sheets across marine margins in subpolar regions increased the sensitivity of the global climate system to obliquity variations at this time. The resulting strengthening of meridional and zonal temperature gradients and shoaling of the tropical thermocline would cause enhanced aridification of East Africa and Arabia, and meanwhile a stronger East Asian winter and summer monsoon. Our study highlights the likely contribution of subpolar sea ice expansion on critical transitions in global climate and ecosystem evolution via its ability to modify the sensitivity of the Earth system to orbital variations.

The mid-Early Pleistocene (1.9–1.6 Ma) witnessed a prominent global climate change, including an increase in global dust fluxes[1–3], intensification of the East Asian monsoon system[4–6], and shifts in global oceanic circulation[7]. In East Africa, there was an ecological shift towards open grassland habitats accompanied by major developments in the hominin clade—including the highest diversity of hominins, the extinction of the Paranthropus lineage and the appearance of our direct ancestor *Homo erectus* at ~1.8 Ma[8–11]. However, external factors controlling the climate system at this time, such as solar insolation, orbital parameters and atmospheric $CO_2$ concentration[12–14] as well as global ice volume variations[15], were relatively stable. This creates an enigma in determining the driving factors for these apparent mid-Early Pleistocene events.

In contrast to the relatively invariant external forcing factors over the early Pleistocene, a prominent increase in the amplitude of Earth's obliquity (i.e., axial tilt, ~41 kyr period) signal is observed at 1.9–1.6 Ma in many paleoclimatic records. This increase in obliquity is recorded in bulk sediment grain size in Chinese loess deposits[4,5], dust records from the North Pacific, East Africa and Arabia[3,8], sea surface temperatures (SST) in the South China Sea[16], North and South Atlantic and South Pacific at mid-latitudes[17,18]. Variations in obliquity can modulate meridional temperature gradients and poleward moisture transport[19,20]. Therefore, one possible hypothesis for the mid-Early Pleistocene intensification of obliquity in paleoclimatic records is that Northern Hemisphere ice sheets[4,5] and/or the Arctic sea ice attained a critical extent[3] that allowed them to significantly influence the East-Asian winter monsoon system. The 41-kyr signal observed in marine sediments of the tropical regions may be derived from obliquity-controlled processes at high latitudes that are transmitted to low latitudes via the atmosphere or ocean circulation[21,22]. Other contributing processes that may have amplified the obliquity signal during the Pliocene-Pleistocene include an enhanced iron fertilization-$CO_2$ feedback[2] and/or an amplified $CO_2$ feedback in conjunction with intensified Northern Hemisphere glaciation[21]. Taken together, an enhanced sensitivity to, or feedback from, the global climate system to obliquity could explain the observed late Early Pleistocene environmental shifts.

[1]Key Laboratory of Green and High-end Utilization of Salt Lake Resources, Qinghai Institute of Salt Lake, Chinese Academy of Sciences, 810008 Xining, China. [2]Shandong Provincial Key Laboratory of Water and Soil Conservation and Environmental Protection, College of Resources and Environment Sciences, Linyi University, 276000 Linyi, China. [3]State Key Laboratory of Tibetan Plateau Earth System Science, Resources and Environment (LTPESRE), Institute of Tibetan Plateau Research, Chinese Academy of Sciences, 100101 Beijing, China. [4]State Key Laboratory for Biogeology and Environmental Geology and Hubei Key Laboratory of Critical Zone Evolution, School of Earth Sciences, China University of Geosciences (Wuhan), Wuhan, China. [5]School of Earth Sciences & Key Laboratory of Western China's Mineral Resources of Gansu Province, Lanzhou University, Lanzhou, China. ✉e-mail: wenxia_han@163.com; zanjb@itpcas.ac.cn

To test this idea, we collated multi-proxy paleoclimate records from a broad region (Fig. 1) spanning the last 2.8 Ma and performed linear and nonlinear analyses of these data. These methods included evolutionary spectral analysis and obliquity sensitivity analysis, as well as recurrence analysis, in order to trace evolutionary patterns in the time and frequency domains. Our results reveal a general synchronous change in temporal variations of all the records started at 1.9–1.6 Ma that corroborate the global environment transition and an increased sensitivity/feedback to obliquity. This is coincident in time with a major subpolar cooling[18,21,23,24]. We thus posit that the mid-Early Pleistocene climate–environment changes were induced by increased sensitivity of the global climate system to obliquity-forced bipolar sea ice expansion.

### Significant changes in the global climate system during the mid-Early Pleistocene

Temporal variations in the Mn flux records in the Qaidam Basin and the South China Sea and in sediment K content in the Sea of Japan[25–28] (Fig. 2b, f, g) (which are closely related to hydroclimate conditions of the Asian interior and eolian dust inputs from continental Asia), show an increase starting at ~1.9 Ma. Dust flux records from pelagic sediments in the Eastern Mediterranean[29], Arabian Sea and Southern Oceans[30] (Fig. 2e, h) exhibit a similar increasing trend at around this time. These observations suggest that a climatic shift toward increased aridity occurred within the African monsoon regions, the Middle Asia and the Asian interior since the mid-Early Pleistocene.

Sediment grain-size data from the Chinese Loess Plateau, which reflects variations in East Asian winter monsoon intensity, reveals a substantial increase in the intensity of the winter monsoon at ~1.7 Ma[4,5]. In addition, a carbonate-based rainfall proxy[6] and the summer monsoon index[31] both indicate an increasing trend in East Asia summer monsoon intensity since ~1.7 Ma (Fig. 2c, d). Overall, these hydroclimate records and monsoon-proxy results imply a shift beginning at ~1.8 Ma to more pronounced aridity with increased dust activity from African-Asian regions, and an increased East Asia summer monsoon accompanied by slightly strengthened East Asia winter monsoon and dust activity in Central Asia.

Coinciding with these major climatic and environmental changes, a consistent system transition is identified at 1.9–1.6 Ma in the recurrence analysis of the studied proxy records from different regions (Fig. 3). In a recurrence plot, deterministic periodic processes are expressed as dark-shaded areas dominated by longer lines and less isolated recurrence points, while chaotic or stochastic fluctuations are expressed as unshaded areas with very short lines or single isolated recurrence points. The transition between different states captures important regime changes within the data[32]. From the recurrence plots for the studied records, we identify four potential regime changes at 2.4−2.1, 1.9−1.6, 1.3−1.1 and ~0.6 Ma (details in Fig. 3 and Supplementary Table 1). It is clear that all the proxy records do not

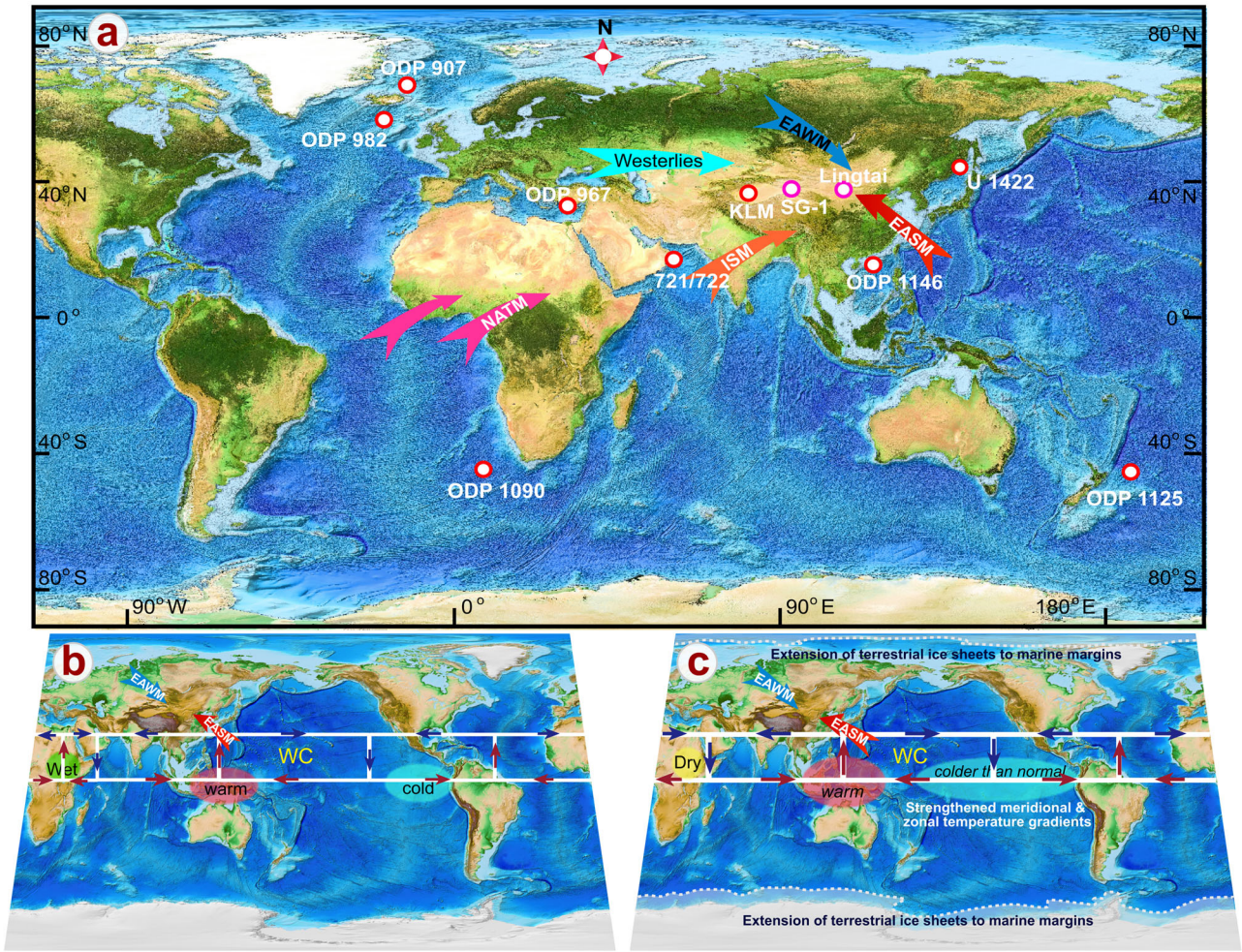


**Fig. 1 | Map showing the locations of study sites and simple schematic models showing the effects of subpolar sea ice expansion. a** Locations of the data used in this study, with principle trajectories of atmospheric circulation also shown. **b**, **c** Schematic illustrations showing the conditions and effects of normal (**b**) and extended (**c**) terrestrial ice sheets across the marine margins in the sub-Antarctic and sub-Arctic regions. EASM East Asian Summer Monsoon, EAWM East Asian Winter Monsoon, ISM Indian Summer Monsoon, NATM North Africa tropic monsoon, WC Walker Circulation.

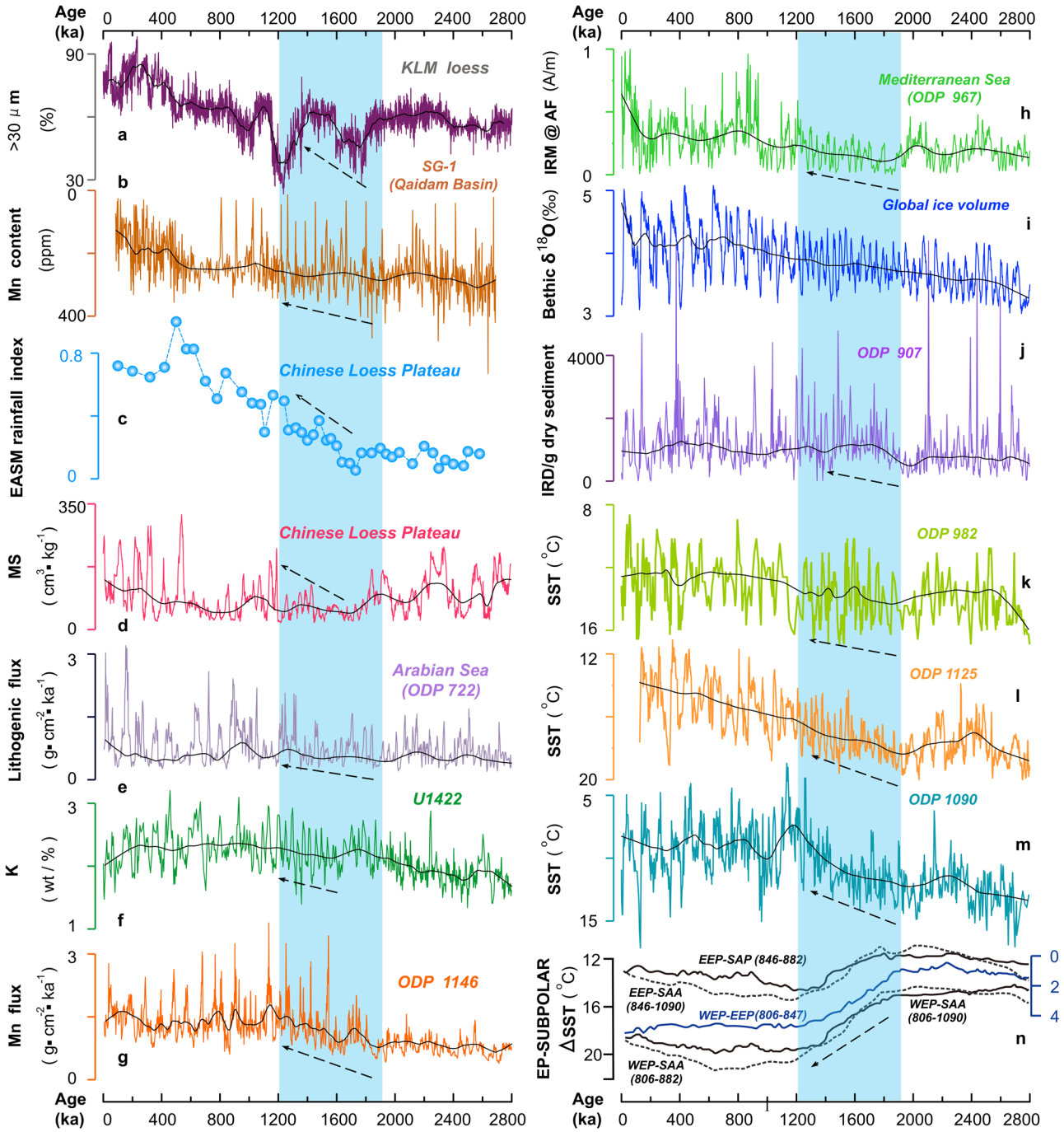


**Fig. 2 | Temporal variations in various paleoclimate proxies across the past 2.8 Myr. a** Coarse sediment size fraction (>30 μm) from the Western Kunlun Mountain[58]. **b**, **g** Mn flux records in the Qaidam Basin[25,26] (SG-1) and South China Sea[27] (ODP Site 1146), respectively. **c**, **d** A carbonate-based rainfall proxy[6] and the summer monsoon index[31] from the Chinese Loess Plateau. **e**, **h** Dust flux records from the Arabian sea[30] (ODP Site 722) and pelagic sediments in Eastern Mediterranean[29] (ODP Site 967), respectively. **f** Sediment K content in the Japan sea[28]. **i** Marine $\delta^{18}O$ data[15]('LR04'). **j** Ice-rafted debris (IRD) record from ODP Site 907 in the Nordic Seas[23]. **k**–**m** SST records of ODP sites 982[21], 1125[17] and 1090[18], respectively. **n** Differences (based on 400-kyr smoothing curves[18]) between SST data to illustrate latitudinal and meridional SST gradients. Data used are ODP sites 846[63] and 847[41] for the eastern equatorial Pacific (EEP), ODP Site 806[41] for the western equatorial Pacific (WEP), ODP Site 1090[18] for the sub-Antarctic Atlantic (SAA) and ODP Site 882[18] for the sub-Arctic Pacific (SAP). Gradients indicated by calculating EEP-SAP, EEP-SAA, WEP-EEP and WEP-SAA. *Note*: Black lines in **a**–**m** show dominant trends based on locally weighted scatterplot smoothing (LOWESS, smoothing factor 0.1).

display exactly the same features, with slight time differences perhaps due to differing resolutions or the various controlling factors on the different proxies. Nevertheless, the regime shift found in some of the datasets at 2.4-2.2 Ma has also been revealed by a nonlinear measure for transition detection on alkenone SST record from ODP Site 722 using recurrence quantification analysis[32] and a newly designed fluctuation of similarity method[33]. This shift was explained as an inter-regime transition, a transition between two different regimes[32]. The regime shift identified in some records at ~1.2 Ma is coincident with the well-known Mid-Pleistocene climate transition (MPT)[32–34] and the regime shift indicated at 0.6–0.4 Ma might be related to an interval when the sensitivity of the high-latitude climate response to solar forcing reached its maximum[32,34,35].

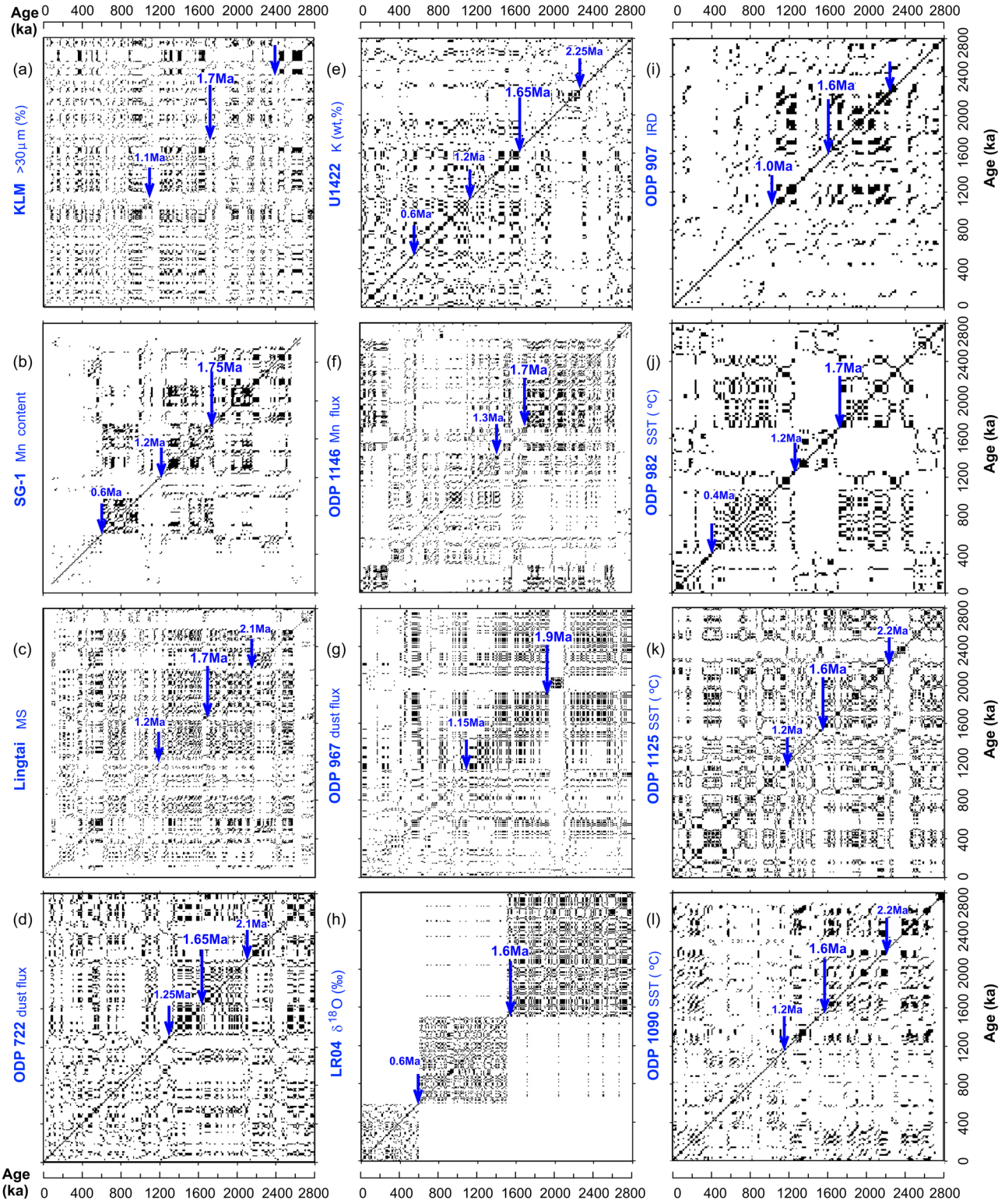


**Fig. 3 | Climate regime shifts revealed by recurrence analysis of global climate and oceanographic records.** Recurrence plots showing patterns of climate change and major system transitions: the coarse size fraction (>30 μm) from the Western Kunlun Mountain (KLM)[58] (**a**), the $Mn_{HOAC}$ data from the Qaidam Basin[25,26] (**b**), the magnetic susceptibility (MS) data from the Chinese Loess Plateau[31] (**c**), the dust flux record from the ODP Site 722 in the Indian Ocean[30] (**d**), the K content from the IODP Site U1422 in the Sea of Japan[28] (**e**), dust flux records from ODP Site 1146 in the South China Sea[27] (**f**) and Site 967 in the Eastern Mediterranean[29] (**g**), and the LR04 marine $\delta^{18}O$ data[15] (**h**), the ice-rafted debris (IRD) record from the ODP Site 907 in the Nordic Seas[23] (**i**) and the SST records of ODP sites 982[21] (**j**), 1125[17] (**k**) and 1090[18](**l**).

Evidence for the regime shift at ~1.9-1.6 Ma seems to be apparent in all our measured datasets, albeit with varying clarity (Fig. 3 and Supplementary Table 1). A climate transition around this time has also been recognized in previous studies using different methods. For example: in Indian monsoon patterns at ~1.9–1.5 Ma, as calculated from the lithogenic grain size record from ODP Site 722B (reflecting the wind intensity of Asian monsoon[30,33]), in the SST record of ODP Site 722 from the Arabian Sea at 1.9-1.7 Ma[32], in the terrestrial dust flux record of ODP sites 659 (East Atlantic), 721/722 (Arabian Sea) and 967 (Eastern Mediterranean Sea) at 1.8–1.6 Ma[36], as well as in eolian variability records in Africa at ~1.7 Ma[8]. This broadly consistent evidence for a regime shift in multiple proxy records corroborates the view that there was a worldwide climate state transition during the mid-Early Pleistocene.

The identification of an environmental transition in the mid–Early Pleistocene contrasts with the relative stability of external forcing factors over this time interval, with little change evident in parameters such as solar insolation and atmospheric $CO_2$ concentration[12–14] (Supplementary Fig. 1). However, the timing of this transition is coeval with a substantial cooling and sea ice expansion in subpolar and high latitudes, as corroborated by a prominent drop of sub-Antarctic and sub-Arctic SST[18], an increase of ice-raft debris in the Nordic Seas[23] and the Feni drift[37], and a prominent drop of SST at high latitudes on both hemispheres based on multiproxy paleotemperature estimates from marine sediments in the sub-Arctic Atlantic and the Southern Oceans[17,18,21,23,24] (Fig. 2j-m).

Evolutionary spectral analysis and calculated obliquity power (O/T) of our studied records indicate an intensification of obliquity energy between 1.9 and ~1.2 Ma (Fig. 4). In addition, the obliquity sensitivity ($S_{obl}$) of the collated records further indicates increased sensitivity of the climate system to obliquity, starting at 1.9–1.6 Ma (Fig. 4). These results are consistent with the work of ref. 17, which showed a similar increase in 41-ka obliquity in several marine $\delta^{18}O$ datasets at 1.8 Ma. Previous work has indicated that terrestrial ice sheets are more sensitive to atmospheric temperature changes modulated by variations in eccentricity and precession, whereas significant increases in $S_{obl}$ would occur when outlet glaciers advanced across terrestrial margins into marine environments, where they then become more sensitive to ocean-driven oscillations influenced by changes in Earth's obliquity[38]. Thus, the intensification of obliquity and the increased obliquity sensitivity ($S_{obl}$) that we observe in the proxy climate records starting at 1.9–1.6 Ma provide supporting evidence for a mechanistic link with coeval cooling and sea ice expansion at subpolar and high latitudes.

To further verify this link, we employed cross-wavelet analysis between dust and monsoon-proxy records and the two hemisphere high latitude SST records from ODP sites 1125[17] (Fig. 5a–g) and 982[21] (Fig. 5h–n). The results show a consistently strong correlation between these datasets at the 41-kyr obliquity period, beginning at 1.9–1.6 Ma. This strong correlation at the obliquity scale supports the strong influence of high latitude SST variations on global dust and monsoon records, and their increased response to obliquity forcing from ~1.9 to ~1.2 Ma. After this, a strong correlation appears between the dust and monsoon records and high latitude SST data at the ~100-kyr short eccentricity period. This likely indicates a response to the MPT event, since it is at this time that global climate records reveal a shift from dominant 41-kyr forcing to dominant ~100 kyr forcing. As noted earlier, this climate shift is also evident in our recurrence analysis (Fig. 3).

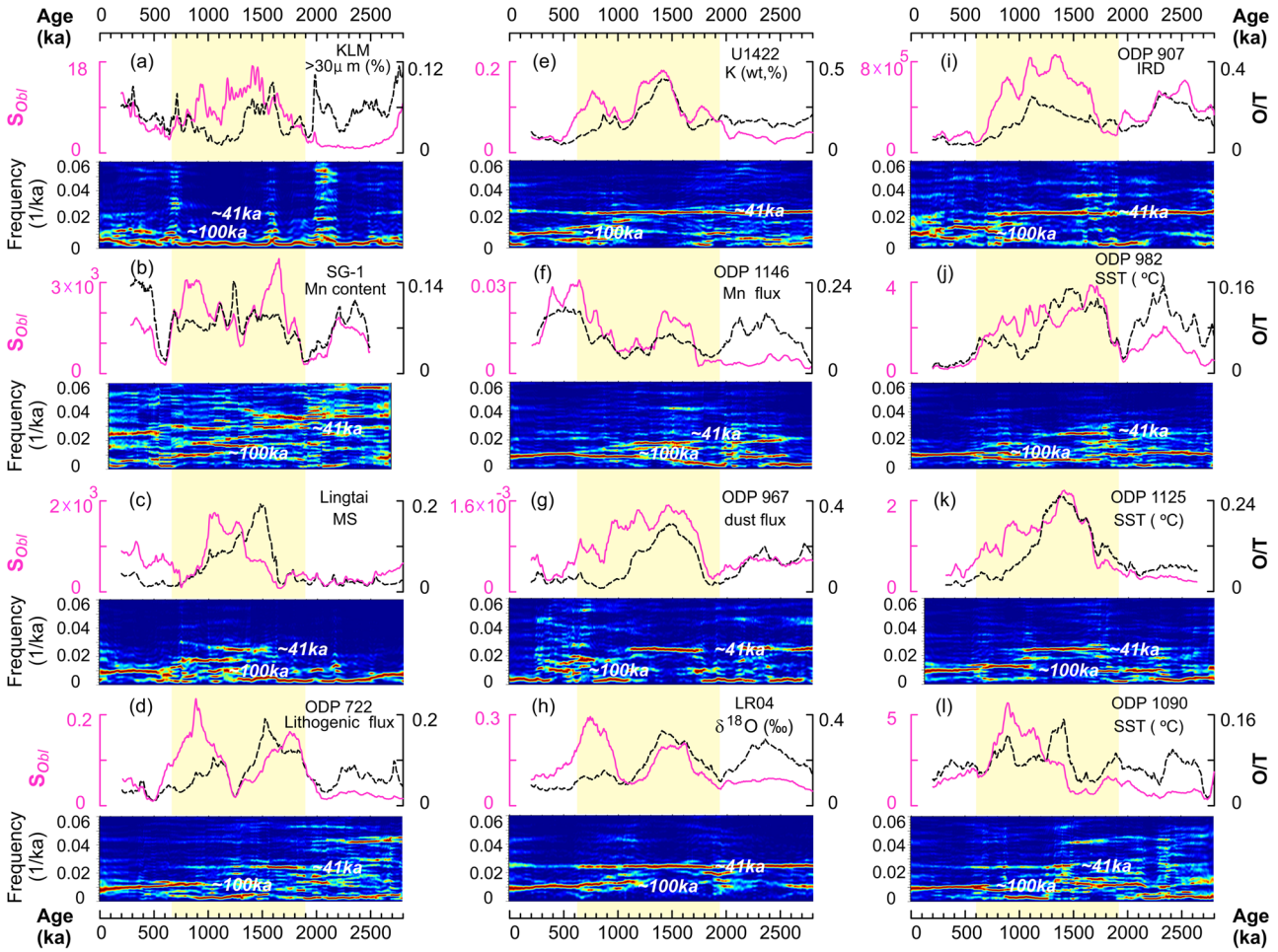


**Fig. 4 | An intensification of obliquity energy between 1.9 and ~1.2 Ma in global climate and oceanographic records.** Obliquity sensitivity ($S_{obl}$; purple curves), the ratio of obliquity to total energy (O/T; black curves) and evolutionary spectrograms of the collated climate records (the data sources in **a** to **l** are same as in Fig. 3).

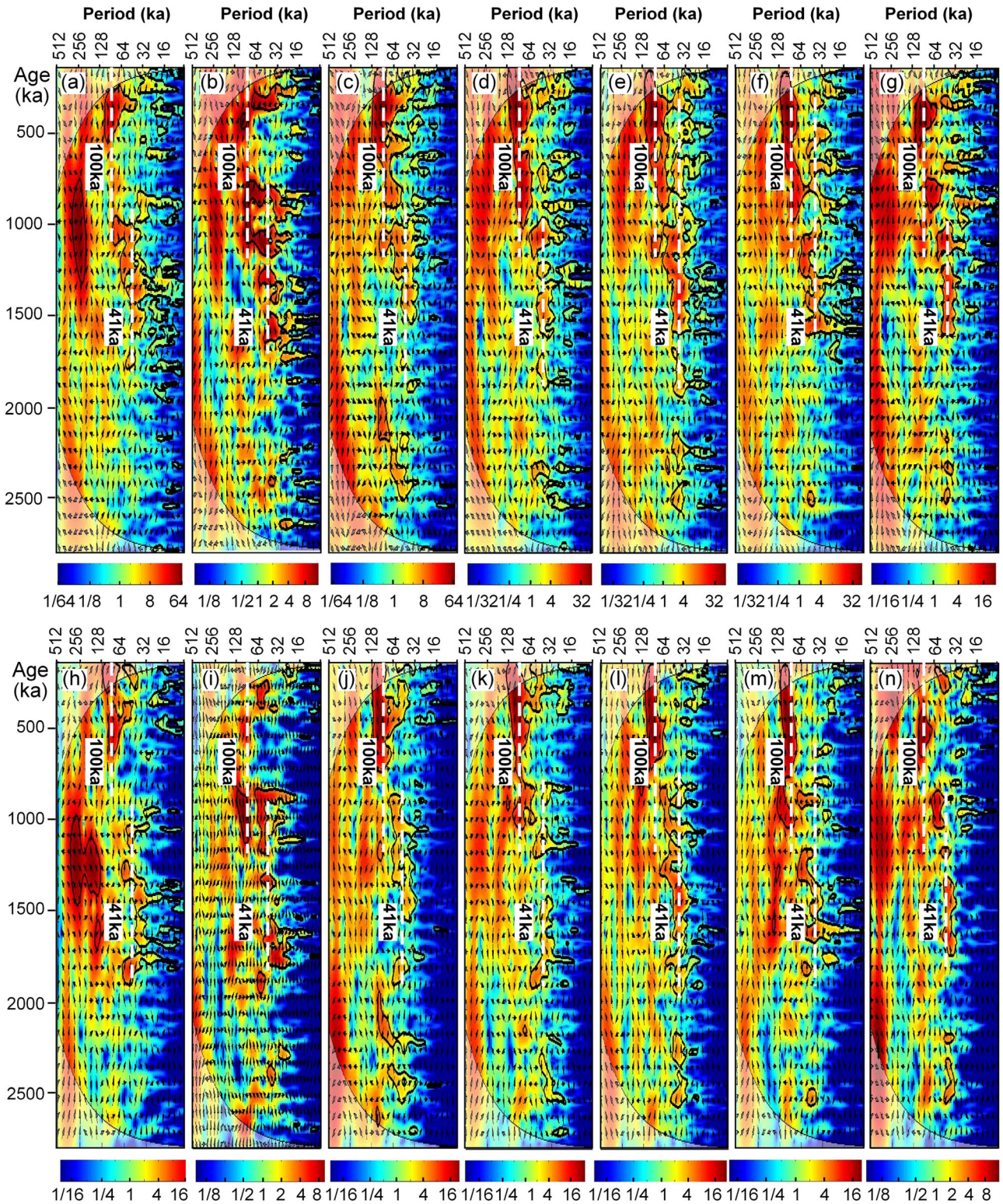


**Fig. 5 | A strong correlation between the global dust and monsoon records and the high latitude SST variations at the obliquity scale.** Cross-wavelet analysis between dust and monsoon-proxy records and two hemispheres high latitude SST records from ODP Site 1125[17] (**a**–**g**), and ODP Site 982[21] (**h**–**n**). Specific dust and monsoon-proxy records used are as follows: the coarse size fraction (>30 μm) from the Western Kunlun Mountain (KLM)[58] (**a**, **h**), the $Mn_{HOAC}$ data from the Qaidam Basin[25,26] (**b**, **i**), the MS data from the Chinese Loess Plateau[31] (**c**, **j**), the dust flux record from the ODP Site 722[30] (**d**, **k**), the K content from the IODP Site U1422[28] (**e**, **l**), the dust flux record from ODP Site 1146[27] (**f**, **m**), and the dust flux record from ODP Site 967[29] (**g**, **n**).

### Subpolar marine ice expansion forced global climate shifts during the late early Pleistocene

The combined evidence indicates that subpolar sea ice expansion drove increased obliquity and contributed to the climatic and environmental transitions during the mid-Early Pleistocene. A bipolar cooling and extension of sea ice range in the sub-Antarctic and sub-Arctic regions might increase the sensitivity of the global climate system to the obliquity beat, thereby imprinting a significant obliquity signal to a wide region through ocean circulation[18,39].

Subpolar sea ice expansion could have facilitated the strengthening of the meridional and zonal temperature gradients (see the schematic model in Fig. 1b and c). Furthermore, it would also induce the increased sensitivity of ice sheets to ocean-driven oscillations influenced by changes in Earth's obliquity[38]. Obliquity can exert a significant influence on the meridional temperature gradient and poleward moisture transport, which are important factors controlling moisture supply to sustain ice sheet growth at high latitudes[19,20]—thus serving as a positive feedback to ice expansion. We note a prominent increase in the meridional temperature gradient between the subpolar regions and the equatorial Pacific[18,40], and enhanced zonal SST gradient along the equator Pacific[18,41] in the mid-Early Pleistocene (Fig. 2n). This would subsequently promote strengthened surface high-pressure zones at low latitudes (subtropical highs), a slightly equatorward contraction and intensification of the Hadley Circulation[19,20,32–44], and a shoaling of the tropical thermocline[45–47], thereby leading to stronger upwelling in subtropical Atlantic and Pacific oceans and the development of the modern cold tongue on the eastern sides of the Pacific and Atlantic basins[18,40,42]. The resulting stronger zonal SST gradient in the Indian Ocean and the stronger coastal upwelling in the Arabian Sea (hence a cooler Arabian Sea) (Fig. 1b, c) may have been responsible for a strengthening of the Asian monsoon through coupling between the winds and SSTs and increased aridification in East Africa[40,48,49]. At the same time, the stronger zonal SST gradient in the Pacific and associated enhanced Walker circulation[18] and mid-latitude Hadley circulation over the West Pacific (Fig. 1b, c) would produce stronger trade winds. These would promote a strengthening of the intensity of the East Asian tropical monsoon trough[50] and the development of anomalous lower-tropospheric cyclones in the western North Pacific, thereby inducing stronger winter[16,50–53] and summer monsoons[50,52] in East Asia.

Our inferred link between cooling-driven ice expansion in subpolar regions and modifications to meridional and zonal temperature gradients (as well as increased sensitivity of the climate system to obliquity), is supported by previous modeling work. For example, experiments on the Plio-Pleistocene climate response to obliquity forcing indicate that a growing Greenland ice sheet will induce an amplified response of the zonal mean atmospheric circulation, the Hadley circulation and the Atlantic Meridional Overturning Circulation variations to obliquity forcing, resulting in a stronger surface air temperature variability[54]. A climate–vegetation–ice sheet model designed to simulate climate-ice sheet responses to transient orbital parameters shows that amplification of obliquity forcing by sea ice, vegetation, and cloud feedback is crucial for explaining the dominant influence of obliquity on Quaternary ice sheets[55]. Simulations also indicate a prominent control of obliquity-driven meridional thermal contrast on the evolution of the East Asian winter[56] and summer[57] monsoons.

Subpolar sea ice expansion and the resulting increased response of the global climate system to obliquity variations would have exerted important effects on climate, environment, and ecosystems in the Middle East and in Central and East Asia. As such, our results may provide an explanation for the observed environment transitions and hominin evolution changes in Africa at 1.9–1.6 Ma[8–11]. This also hints at an implication for future global climate change predictions, and that attention should be paid to the impact of variations in sea surface temperature and sea ice extent in the subpolar regions on the sensitivity of the global climate system to orbital parameters.

Linear and nonlinear analyses on collated climate- and oceanographic-proxy records indicate a global climatic and environmental transition contemporaneous with strengthened sensitivity to orbital obliquity variations at 1.9-1.6 Ma. The array of globally distributed records we present suggests that the increased sensitivity to obliquity during this mid-Early Pleistocene interval was linked to a coeval bipolar cooling and prominent ice expansions in the subpolar regions. These would have caused feedback on the strength of meridional temperature gradients and, in turn, a shoaling of the tropical thermocline. The resulting stronger Hadley circulation over the West Pacific and related stronger trade winds could have been important contributors to the enhanced aridification of East Africa and Arabia and to stronger East Asian winter and summer monsoons, thereby inducing the observed critical transitions in global climate, ecosystems and associated hominin evolution at around this time. Our study highlights the importance of variations in the sea surface temperature and ice extent in the subpolar regions and their impacts on modulating the sensitivity of the global climate system to different orbital forcing.

## Methods

### Data sources

We compiled multi-proxy records worldwide for analysis and comparison (Fig. 2). The data comprise: (1) coarse size fraction (>30 μm) of a long drill core record of loess from the Western Kunlun Mountain[58], which is considered a proxy for wind strength, (2) magnetic susceptibility data from the Chinese Loess Plateau, which is an indicator of the intensity of the Asian summer monsoon[31], (3) acetic acid-leached manganese content ($Mn_{HOAC}$) data[25,26] of a long borehole from the Qaidam Basin, (4) K content from IODP Site U1422 in the Japan sea[28], and (5) dust flux records from the ODP sites 1146 in South China Sea[27], 967 in Eastern Mediterranean[29] and 722 in Indian Ocean[30]. Together, these data can be used to identify temporal variations in dust supply and paleoenvironmental evolution in the Asia interior, North Africa and the Middle East. In addition, SST data from ODP sites 982[21], 1125[17] and 1090[18] have been used, as well as an ice-rafted debris (IRD) record from ODP Site 907 in the Iceland Sea[23] that can reveal dynamic sea-ice expansion and oceanic circulation processes.

### Obliquity sensitivity

The obliquity sensitivity ($S_{obl}$) is calculated following the method of Levy et al. (2019)[38], in which $S_{obl}$ is defined as $\delta^2_{proxy}/\delta^2_{La04}$, where $\delta^2_{proxy}$ is the obliquity variance of the paleoclimatic proxy under investigation, and the $\delta^2_{La04}$ is the theoretical obliquity variance based on data from ref. 13. Multitaper time-frequency power spectra were used to quantify the $S_{obl}$ through time, and was based on integration of variance between 0.023 and 0.027 cycles/kyr (i.e., 43–37 kyr) in order to obtain the dominant 41 kyr obliquity signal. A 400 kyr window and a 10 kyr time step were used.

### Obliquity power calculation

The power (i.e. variance) of obliquity (O) in the individual proxies was calculated by integrating spectra in the frequency band 1/37–1/43 kyr, and dividing this power by the total power ($T$) integrated from 0 to the Nyquist frequency. A $2\pi$ multi-taper evolutionary spectral analysis with a 400-kyr sliding window was used to track obliquity power through time[59]. The evolutionary spectral analysis was performed using evolutionary fast Fourier transform spectrograms with a 400-kyr window[60].

### Recurrence analysis

To detect potential nonlinear dynamical transitions in proxy data, a recurrence analysis was conducted. Recurrence analysis identifies the extent to which the studied system can 'repeat' itself and thus provides independent information on nonlinear dynamics and dynamical transitions[61]. In a recurrence plot, periodic processes are expressed as dark-shaded areas dominated by longer lines and less isolated recurrence points, while chaotic or stochastic fluctuations are expressed as unshaded areas with very short lines or single isolated recurrence points. The transition between different states captures important regime changes within the data[61]. The original unevenly spaced data were preprocessed using the Transformation Cost Time Series method[62]. The recurrence analysis was performed following the method of ref. 61 with an adaptively chosen threshold distance that ensures a constant recurrence rate of 10%.

## Data availability

All data are available through refs. 18,25–31,58,63 and are publicly available from the website at: https://www.ncei.noaa.gov/products/paleoclimatology.

Received: 31 October 2023; Accepted: 2 February 2024;
Published online: 17 February 2024

## References

1. deMenocal, P. B. African climate change and faunal evolution during the Pliocene–Pleistocene. *Earth Planet. Sci. Lett.* **220**, 3–24 (2004).
2. Martínez-Garcia, A. et al. Southern Ocean dust–climate coupling over the past four million years. *Nature* **476**, 312–315 (2011).
3. Cao, M. et al. Mineral dust coupled with climate–carbon cycle on orbital timescales over the past 4 Ma. *Geophys. Res. Lett.* **48**, e2021GL095327 (2021).
4. Liu, T. & Ding, Z. Chinese loess and the paleomonsoon. *Annu. Rev. Earth Planet. Sci.* **26**, 111–145 (1998).
5. Liu, T., Ding, Z. & Rutter, N. Comparison of Milankovitch periods between continental loess and deep sea records over the last 2.5 Ma. *Quat. Sci. Rev.* **18**, 1205–1212 (1999).
6. Meng, X. et al. Mineralogical evidence of reduced East Asian summer monsoon rainfall on the Chinese loess plateau during the early Pleistocene interglacials. *Earth Planet. Sci. Lett.* **486**, 61–69 (2018).
7. Wang, P. X. et al. Long-term cycles in the carbon reservoir of the Quaternary ocean: a perspective from the South China Sea. *Natl Sci. Rev.* **1**, 119–143 (2014).
8. deMenocal, P. B. Plio-Pleistocene African climate. *Science* **270**, 53–59 (1995).
9. Maslin, M. A., & Trauth, M. H. Plio-Pleistocene East African pulsed climate variability and its influence on early human evolution. In *The First Humans—Origin and Early Evolution of the Genus Homo* (eds Grine, F. E., Fleagle, J. G., Leakey, R. E.) *Vertebrate Paleobiology and Paleoanthropology* (Springer, Dordrecht, 2009).
10. Cerling, T. E. et al. Woody cover and hominin environments in the past 6 million years. *Nature* **476**, 51–56 (2011).
11. Maslin, M. A. et al. East African climate pulses and early human evolution. *Quat. Sci. Rev.* **101**, 1–17 (2014).
12. Berger, A. & Loutre, M. F. Insolation values for the climate of the last 10 million years. *Quat. Sci. Rev.* **10**, 297–317 (1991).
13. Laskar, J. et al. Long term evolution and chaotic diffusion of the insolation quantities of mars. *Icarus* **170**, 343–364 (2004).
14. Rae, J. W. B. et al. Atmospheric $CO_2$ over the past 66 million years from marine archives. *Annu. Rev. Earth Planet. Sci.* **49**, 609–641 (2021).
15. Lisiecki, L. E. & Raymo, M. A. Pliocene–Pleistocene stack of 57 globally distributed benthic $\delta^{18}O$ records. *Paleoceanogr. Paleoclimatol.* **20**, PA1003 (2005).
16. Li, D., Zhao, M. & Tian, J. Low-high latitude interaction forcing on the evolution of the 400 kyr cycle in East Asian winter monsoon records during the last 2.8 Myr. *Quat. Sci. Rev.* **172**, 72–82 (2017).
17. Peterson, L. C. et al. Plio-Pleistocene hemispheric (A)symmetries in the Northern and Southern Hemisphere midlatitudes. *Paleoceanogr. Paleoclimatol.* **35**, e2019PA003720 (2020).
18. Martínez-Garcia, A., Rosell-Melé, A., McClymont, E. L., Gersonde, R. & Haug, G. H. Subpolar link to the emergence of the modern equatorial Pacific cold tongue. *Science* **328**, 1550–1553 (2010).
19. Raymo, M. E., & Nisancioglu, K. H. The 41 kyr world: Milankovitch's other unsolved mystery. *Paleoceanogr. Paleoclimatol*. **18**, 1011 (2003).
20. Huybers, P. & Wunsch, C. Obliquity pacing of the late Pleistocene glacial terminations. *Nature* **434**, 491–494 (2005).
21. Herbert, T. D. et al. Late Miocene global cooling and the rise of modern ecosystems. *Nat. Geosci.* **9**, 843–847 (2016).
22. Liu, Z. & Herbert, T. D. High-latitude influence on the eastern equatorial Pacific climate in the early Pleistocene epoch. *Nature* **427**, 720–723 (2004).
23. Jansen, E., Fronval, T., Rack, F. & Channell, J. E. T. Pliocene–Pleistocene ice rafting history and cyclicity in the Nordic Seas during the last 3.5 Myr. *Paleoceanogr. Paleoclimatol.* **15**, 709–721 (2000).
24. Lawrence, K. T., Sosdian, S., White, H. E. & Rosenthal, Y. North Atlantic climate evolution through the Plio–Pleistocene climate transitions. *Earth Planet. Sci. Lett.* **300**, 329–342 (2010).
25. Yang, Y. et al. Late Pliocene–Quaternary evolution of redox conditions in the western Qaidam paleolake (NE Tibetan Plateau) deduced from Mn geochemistry in the drilling core SG-1. *Quat. Res.* **80**, 586–595 (2013).
26. Yang, Y. et al. Glacial-interglacial climate change on the northeastern Tibetan Plateau over the last 600 kyr. *Palaeogeogr. Palaeoclimatol. Palaeoecol.* **476**, 181–191 (2017).
27. Clemens, S. C., Prell, W. L., Sun, Y., Liu, Z. & Chen, G. Southern hemisphere forcing of Pliocene $\delta^{18}O$ and the evolution of Indo-Asian monsoons. *Paleoceanogr. Paleoclimatol*. **23**, PA4210 (2008).
28. Zhang, W., De Vleeschouwer, D., Shen, J., Zhang, Z. & Zeng, L. Orbital time scale records of Asian eolian dust from the Sea of Japan since the early Pliocene. *Quat. Sci. Rev.* **187**, 157–167 (2018).
29. Larrasoaña, J. C., Roberts, A. P., Rohling, E. J., Winklhofer, M. & Wehausen, R. Three million years of monsoon variability over the northern Sahara. *Clim. Dyn.* **21**, 689–698 (2003).
30. Clemens, S. C., Murray, D. W. & Prell, W. L. Nonstationary phase of the Plio–Pleistocene Asian Monsoon. *Science* **274**, 943–948 (1996).
31. Sun, Y., An, Z., Clemens, S. C., Bloemendal, J. & Vandenberghe, J. Seven million years of wind and precipitation variability on the Chinese Loess Plateau. *Earth Planet. Sci. Lett.* **297**, 525–535 (2010).
32. Marwan, N., Schinkel, S. & Kurths, J. Recurrence plots 25 years later—gaining confidence in dynamical transitions. *Europhys. Lett.* **101**, 20007 (2013).
33. Malik, N., Zou, Y., Marwan, N. & Kurths, J. Dynamical regimes and transitions in Plio–Pleistocene Asian monsoon. *Europhys. Lett.* **97**, 40009 (2012).
34. Han, W. X. et al. Climate transition in the Asia inland at 0.8–0.6 Ma related to astronomically forced ice sheet expansion. *Quat. Sci. Rev.* **248**, 106580 (2020).
35. Ravelo, A. C., Andreasen, D. H., Lyle, M., Olivarez Lyle, A. & Wara, M. W. Regional climate shifts caused by gradual global cooling in the Pliocene epoch. *Nature* **429**, 263–267 (2004).
36. Donges, J. F. et al. Nonlinear detection of paleoclimate-variability transitions possibly related to human evolution. *Proc. Natl Acad. Sci. USA* **108**, 20422–20427 (2011).
37. McIntyre, K., Ravelo, A. C. & Delaney, M. L. North Atlantic intermediate waters in the late Pliocene to early Pleistocene. *Paleoceanogr. Paleoclimatol.* **14**, 324–335 (1999).
38. Levy, R. H. et al. Antarctic ice-sheet sensitivity to obliquity forcing enhanced through ocean connections. *Nat. Geosci.* **12**, 132–137 (2019).
39. Ai, X. E. et al. Southern Ocean upwelling, Earth's obliquity, and glacial-interglacial atmospheric $CO_2$ change. *Science* **370**, 1348–1352 (2020).
40. Brierley, C. M. & Fedorov, A. V. Relative importance of meridional and zonal sea surface temperature gradients for the onset of the ice ages and Pliocene–Pleistocene climate evolution. *Paleoceanogr. Paleoclimatol.* **25**, PA2214 (2010).
41. Wara, M. W., Ravelo, A. C. & Delaney, M. L. Permanent El Niño-like conditions during the Pliocene warm period. *Science* **309**, 758–761 (2005).
42. Brierley, C. M. et al. Greatly expanded tropical warm pool and weakened Hadley circulation in the early Pliocene. *Science* **323**, 1714–1718 (2009).

43. Etourneau, J., Schneider, R., Blanz, T. & Martinez, P. Intensification of the Walker and Hadley atmospheric circulations during the Pliocene-Pleistocene climate transition. *Earth Planet. Sci. Lett.* **297**, 103–110 (2010).
44. Fedorov, A. V., Brierley, C. M. & Emanuel, K. Tropical cyclones and permanent El Niño in the early Pliocene epoch. *Nature* **463**, 1066–1070 (2010).
45. Fedorov, A. V. et al. The Pliocene paradox (mechanisms for a permanent El Niño). *Science* **312**, 1485–1489 (2006).
46. Steph, S. et al. Early Pliocene increase in thermohaline overturning: a precondition for the development of the modern equatorial pacific cold tongue. *Paleoceanogr. Paleoclimatol.* **25**, PA2202 (2010).
47. Ford, H. L., Ravelo, A. C. & Hovan, S. A deep Eastern Equatorial Pacific thermocline during the early Pliocene warm period. *Earth Planet. Sci. Lett.* **355–356**, 152–161 (2012).
48. Fedorov, A. V. et al. Patterns and mechanisms of early Pliocene warmth. *Nature* **496**, 43–49 (2013).
49. Van der Lubbe, H. et al. Indo-Pacific Walker circulation drove Pleistocene African aridification. *Nature* **598**, 618–623 (2021).
50. Zhang, Q. & Tao, S. Tropical and subtropical monsoon over East Asia and its influence on the rainfall over eastern China in summer. *Q. J. Appl. Meteorol.* **9**, 17–23 (1998).
51. Chen, W., Hans, -F. G. & Huang, R. The interannual variability of East Asian winter monsoon and its relation to the summer monsoon. *Adv. Atmos. Sci.* **17**, 48–60 (2000).
52. Wang, B., Wu, R. & Fu, X. Pacific-East Asian teleconnection: how does ENSO affect East Asian climate? *J. Clim.* **13**, 1517–1536 (2000).
53. Zheng, X. et al. ITCZ and ENSO pacing on East Asian winter monsoon variation during the Holocene: sedimentological evidence from the Okinawa trough. *J. Geophys. Res*. **119**, 4410–4429 (2014).
54. Song, Z., Latif, M. & Park, W. Expanding Greenland ice sheet enhances sensitivity of Plio-Pleistocene climate to obliquity Forcing in the Kiel climate model. *Geophys. Res. Lett.* **44**, 9957–9966 (2017).
55. Tabor, C. R., Poulsen, C. J. & Pollard, D. How obliquity cycles powered early Pleistocene global ice-volume variability. *Geophys. Res. Lett.* **42**, 1871–1879 (2015).
56. Shi, Z. G. et al. Distinct responses of East Asian summer and winter monsoons to astronomical forcing. *Clim*. **7**, 1363–1370 (2011).
57. Wu, C. H., Lee, S. Y., Chiang, J. C. H. & Hsu, H. H. The influence of obliquity in the early Holocene Asian summer monsoon. *Geophys. Res. Lett.* **43**, 4524–4530 (2016).
58. Fang, X. et al. The 3.6-Ma aridity and westerlies history over midlatitude Asia linked with global climatic cooling. *Proc. Natl Acad. Sci. USA* **117**, 24729–24734 (2020).
59. Li, M. et al. Obliquity-forced climate during the Early Triassic hothouse in China. *Geology* **44**, 623–626 (2016).
60. Li, M., Hinnov, L. & Kump, L. Acycle: time-series analysis software for paleoclimate research and education. *Comput. Geosci.-Uk.* **127**, 12–22 (2019).
61. Marwan, N., Romano, M. C., Thiel, M. & Kurths, J. Recurrence plots for the analysis of complex systems. *Phys. Rep.* **438**, 237–329 (2007).
62. Eroglu, D. et al. See-saw relationship of the Holocene East Asian-Australian summer monsoon. *Nat. Commun.* **7**, 12929 (2016).
63. Lawrence, K. T., Liu, Z. & Herbert, T. D. Evolution of the eastern equatorial Pacific through Plio-Pleistoceneglaciation. *Science* **312**, 79–83 (2006).


## Acknowledgements

This study was co-supported by the Second Tibetan Plateau Scientific Expedition and Research program (grants 2019QZKK0707 and 2019QZKK0602), the National Science Foundation of China (grants 42071111, 42272112), the Taishan Scholars Program of Shandong (tsqn201812102). We gratefully acknowledge Dr. James Ogg (IUGS Deep-time Digital Earth and Purdue University) for initial editing and suggestions on an early draft of the text, Xiangyu Liu for meaningful discussion.

## Author contributions

W.H.: Conceptualization, investigation, formal analysis, writing—original draft; J.Z.: Writing- original draft, writing—reviewing & editing; D.K.: Writing—reviewing & editing; T.Z.: Writing—reviewing & editing; Z.W.: Formal analysis, writing—reviewing & editing; L.M.: Investigation, formal analysis; X.F.: Writing—reviewing & editing.

## Competing interests

The authors declare no competing interests.

## Additional information

**Supplementary information** The online version contains supplementary material available at https://doi.org/10.1038/s41612-024-00589-2.

**Correspondence** and requests for materials should be addressed to Wenxia Han or Jinbo Zan.